WHIRL MEASUREMENTS ON LEAKAGE FLOWS IN TURBOMACHINE MODELS*

A.J. Addlesee, D. Altiparmak, and S. Pan
Heriot-Watt University
Edinburgh, United Kingdom

59-34
12853
P-12

The beneficial effects claimed for whirl control devices demonstrate that the dynamic behaviour of rotors is influenced by the fluid whirl in shaft and balance drum seals. The present paper reports results from two series of experiments, the first on the factors affecting the whirl at the seal inlet, and the second on the variation of whirl velocity along the seal. In both cases the LDA measurement technique required the clearance between the fixed and rotating parts of the models to be substantially greater than occurs in real machines, but the results are indicative nevertheless. Experimental and theoretical results are given for the radial distribution of whirl velocity in the gap between impeller shroud and pump casing. Results of tests with modified stator surfaces are also shown. This work leads naturally into the second series of experiments where some preliminary measurements of velocity distribution in the clearance between a fixed stator and a rotating shaft are reported for a range of inlet whirl conditions.

NOTATION

C_Q	Flow parameter $Q/\Omega R^2 h$
f	Friction factor
h	Clearance gap size
k	Constant
Q	Leakage flow towards axis
R	Impeller radius
r	Radial coordinate
t	Time
U	Mean axial velocity in annulus
v	Tangential velocity
v_f	Friction velocity
z	Axial coordinate
ε	Eddy kinematic viscosity
ν	Kinematic viscosity
ρ	Fluid density
τ	Shear stress
Ω	Angular velocity of impeller
ω	Angular velocity of fluid

Suffices

1	Impeller shroud surface
2	Surface opposite to impeller shroud
D	Edge of balance drum
R	Edge of impeller
S	Shaft surface

* The work reported here was partially supported by Weir Pumps Ltd.

INTRODUCTION

The part played by fluid whirl in determining the stiffness characteristics of shaft and balance drum seals is widely acknowledged (1,2,3,4). The present report applies particularly to the situation at the high pressure end of a multi-stage centrifugal pump, where a small fraction of the flow leaving the last impeller leaks away through the shaft or balance drum seal. The diameters of shaft, drum and impeller are typically in the ratios 1:2:3 and the leakage path is shown schematically in Fig.1.

For both experimental and analytical purposes the arrangement shown in Fig.1 can be conveniently investigated in two obvious sections, firstly the whirling radial inflow between the impeller shroud and the casing, and secondly the whirling axial outflow through the seal. The stiffness characteristics are determined by events in the seal, but the radial flow in the gap between shroud and casing is important because it influences the whirl of the leakage flow at entry to the annular seal. A number of whirl control devices have been found to have beneficial effects on rotor stability (5,6,7), thus demonstrating the inaccuracy of earlier theories in which the flow entering the seal was supposed to acquire instantly a whirl velocity independent of the entry value.

When a rotor surrounded by fluid in a small clearance gap moves off-centre, it experiences a force which depends on both the position and the translation velocity of the shaft centre, and which has both radial and tangential components. In particular, Black et al (1) showed that a radial displacement produced a tangential force component dependent on the fluid whirl velocity. The interaction between rotor and fluid is clearly extremely complex, and one way to simplify the problem of computing rotor motion is to make some plausible assumption about the variation of whirl along the seal. The force on the shaft is then obtained by integration of the contributions from all the axial elements of the seal, each depending on the assumed local whirl velocity of the fluid. The proposal of Black and co-workers for an asymptotic approach towards a limiting value of whirl appears to be a useful development beyond the discredited step change at entry mentioned above.

Obvious difficulties arise with this approach when the rotor and seal do not have a concentric equilibrium position and fluid particles experience different conditions on their passage through the seal. In some cases the short bearing assumption may be invoked to justify treating the whirl velocity as independent of angular position, but experimental evidence is hard to find.

IMPELLER/CASING FLOW

The angular velocity of the flow leaving the impeller and entering the gap between shroud and casing is typically about half that of the shaft, although it can be much higher under low flow conditions. The clearance gap is several millimetres wide and the situation may be regarded as a steady axi-symmetric flow provided that shaft misalignment and bending do not cause significant angular or temporal variations in the clearance. The flow will be

virtually unaffected by very small amplitude orbital motion of the shaft and, although a number of recent papers have applied CFD technology to the problem (8,9,10), a simple one-dimensional analysis of the flow provides considerable insight.

The Reynolds number ($\Omega rh/\nu$) is typically in excess of 5000 in the seal and at least an order of magnitude higher at the edge of the impeller. At these levels it is reasonable to treat the angular velocity ω as a function of radius r only, although it must in fact reach Ω on the impeller shroud and zero on the casing. The boundary layer thickness on the walls is assumed to be thin and the velocity step adjacent to the wall is combined with a friction factor to approximate the shear stress transmitted to the fluid. The variation of ω with r which results from such an analysis may be regarded as as a balance between extreme cases.

At one extreme, if friction is negligible the angular momentum of the fluid will be conserved as it approaches the axis. In this case:

$$\omega \cdot r^2 = \text{constant} = \omega_R \cdot R^2 \qquad (1)$$

and, using the typical values mentioned above, the angular velocity at the entry to a drum seal would be:

$$\omega \propto (\Omega/2)\cdot(3/2)^2 > \Omega. \qquad (2)$$

The value would of course be much higher for a shaft seal of smaller diameter.

An alternative extreme form of behaviour would result if wall friction dominated the flow instead of being negligible, so that at all radii:

$$f_1 \cdot (\Omega_1-\omega)^2 = f_2 \cdot (\omega-\Omega_2)^2. \qquad (3)$$

Here suffix 1 refers to the impeller shroud so that Ω_1 equals the shaft speed Ω, and suffix 2 refers to the opposite surface. Where surface 2 is the casing, Ω_2 is zero and equation (3) becomes:

$$f_1 \cdot (\Omega-\omega)^2 = f_2 \cdot \omega^2 \qquad (4)$$

whence:

$$\omega = \Omega/(1+(f_2/f_1)^{0.5}) \qquad (5)$$

and, if the friction factors are equal, the outcome is half-speed whirl. For the section of the gap where the opposite surface is the end of the balance drum:

$$\omega = \Omega_1 = \Omega_2 = \Omega.$$

These two extreme cases of angular velocity distribution are illustrated in Fig.2, where it is worth noting that in the dominant friction case the influence of the inlet whirl is confined to a region very close to the impeller edge. As observed in (10), the situation may occur where the high shear stresses, produced by high relative velocities near the outer edge of the impeller shroud, drive the angular velocity close to half-speed whirl (for equal friction factors). But closer to the seal entry where the relative velocities are lower and the fluid residence time is shorter, the tendency to conserve angular momemtum can be expected to assert itself with a consequent rapid rise in whirl velocity. This event is shown as a dashed line on Fig.2.

The whirl profile occurring in any real case is modified by further effects which theoretical work may need to account for. Two mechanisms tend to reduce variations of angular velocity. The first operates by the action of viscosity which produces tangential shear stress between adjacent annular elements of fluid, and the second is the turbulent momentum exchange between elements usually described as Reynolds shear stress. Viscous stress is neglected in the present analysis.

A further effect arises from the secondary flows adjacent to the boundaries. The whirl approaches Ω in the thin fluid layer next to the impeller shroud and, as this is normally faster than the main flow at the same radius, the faster moving fluid tends to move outwards. Similarly the slow-moving fluid next to the fixed boundary tends to move inwards. In cases where the leakage flow is zero or small, these secondary flows can be an important means of transporting angular momentum in the radial direction. The transport is always outwards, whatever the gradient of the main whirl profile. The effect of secondary flows will be small at higher leakage rates except where the net radial flow is zero, in the region :

$$r_S < r < r_D.$$

RADIAL FLOW RIG

Fig.3 shows the arrangement of the test rig used to investigate radial inwards flow. The vertical shaft carries two discs, one 200mm diameter representing the impeller shroud, and a smaller one representing the end of the balance drum. The inlet to the seal is represented by the clearance between the edge of the small disc and an annular plate representing the pump casing. Spacers on the shaft can be changed to vary the effective shaft diameter and the gap between the discs. The test liquid is water and the valves on two pumped loops are used to control the simulated leakage flow and its whirl as it enters the gap at the edge of the large disc. The whirl is induced by the outflow from a whirl chamber with a number of tangential inlets.

The flow is viewed through the sides of the glass-walled containing tank. Velocity measurements are made by forward scatter laser doppler anemometry with the optical axis of the LDA system passing horizontally through the gap between the discs. The beam intersection can be moved on three axes, but direct measurement of the whirl component of velocity by placing the optical axis along a disc diameter is unfortunately obstructed by the shaft. Velocity components have to be computed from measurements at off-diameter positions of the optical axis.

RADIAL FLOW RESULTS

Typical velocity distributions of whirl across the gap width are shown in Fig.4, where the angular velocity is virtually uniform except for thin layers on the walls. These findings provide justification for restricting most further measurements to the mid-plane of the gap and also for a one-dimensional analysis. The Reynolds numbers given on the figures are values of $\Omega R^2/\nu$.

Whirl profiles for a series of tests in which only the flow

rate Q was varied are shown in Fig.5. Increasing the flow rate alters the balance between frictional and inertial effects by increasing the rate at which angular momentum is convected into the gap. The result is a general increase in whirl velocity.

Fig.6 shows the effect on the whirl profile of modifying the stator surface with other controlled variables held constant. The highest line is the standard nominally smooth surface and the dashed line shows the effect of a replacement surface with blind holes 3mm dia × 3mm deep on a 7mm pitch. The other two curves were obtained for stators with twenty-four radial slots 6mm wide extending out to 0.76 × impeller radius. It may be seen that these last results diverge significantly from the smooth surface result only downstream of this radius.

RADIAL FLOW THEORY

A one-dimensional computer model was written to solve the whirl profile, based on the angular momentum equation for an annular element of axial height h and infinitesimal radial extent:

$$r^3 \cdot \partial\omega/\partial t = Q/2\pi h \cdot \partial(r^2\omega)/\partial r + r^2(\tau_2-\tau_1)/\rho h - \partial(r^2\tau/\rho)/\partial r. \qquad (6)$$

Shear stresses τ_1 and τ_2 are applied to the flow by the opposing walls:

$$\tau_1/\rho = f_1 \cdot r^2(\Omega_1-\omega)(\Omega_1\sim\omega)/2 \qquad (7)$$

$$\text{and} \quad \tau_2/\rho = f_2 \cdot r^2(\omega-\Omega_2)(\omega\sim\Omega_2)/2 \qquad (8)$$

where "~" denotes the positive difference between two quantities. The Reynolds stress τ, acting on the interface between adjacent elements can be written as the product of an effective viscosity and the velocity gradient:

$$\tau = -\rho\varepsilon r \cdot \partial\omega/\partial r. \qquad (9)$$

In reality ε will vary across the gap in some way such as:

$$\varepsilon = k(v_{f1} + v_{f2}) \cdot z(h-z)/h \qquad (10)$$

which at least ensures that it is zero on both walls and gives a mean value for use in eq. (9) as:

$$\bar{\varepsilon} = (kh)(v_{f1} + v_{f2})/6. \qquad (11)$$

Each friction velocity can be related to the friction factor on the corresponding wall and the relative velocity. Thus, considering rotational velocities only:

$$v_{f1}^2 = (f_1/2)[(\Omega_1\sim\omega)r]^2 \quad \text{and} \quad v_{f2}^2 = (f_2/2)[(\omega\sim\Omega_2)r]^2 \qquad (12)$$

which allows $\bar{\varepsilon}$ to be written as:

$$\bar{\varepsilon} = kh/6 \cdot \Omega r(f/2)^{0.5} \quad \text{where} \quad f^{0.5}\Omega = f_1^{0.5}(\Omega_1\sim\omega) + f_2^{0.5}(\omega\sim\Omega_2). \qquad (13)$$

The friction factors may be treated as constants or as functions of a local Reynolds number.

Using equation (6) to follow the progress of the transient from an arbitrary initial whirl profile can be made the basis of a numerical solution method. The accuracy of following the transient does not affect the steady-state solution. The equation can be

conveniently made dimensionless by using R and Ω as reference quantities so that ω/Ω becomes ω, r/R becomes r, and Ωt becomes the shaft rotation angle from the start of the transient. If differentiation is denoted by a dash for radius and a dot for angle, equation (6) can be written in dimensionless form as:

$$r^3\dot{\omega} = (Q/2\pi\Omega R^2 h)\cdot(r^2\omega)' - r^2\cdot(\tau_2-\tau_1)/\rho\Omega^2 Rh - (r^2\cdot\tau/\rho\Omega^2 R^2)'. \quad (14)$$

The upper limit on the angular step required to avoid numerical instability in the discretised form of this equation with 20-30 radial steps is typically 5-30 degrees. There is a rapid approach to within a few per cent of the steady state solution in the region where $r>r_D$, but further progress is then limited by slow convergence in the diffusion-controlled region near the shaft where $r<r_D$.

Figs. (7,8) are whirl predictions typical of actual machines and the test rig, which show similar behaviour to the experimental results. A feature observed in some of the test flows is a region of positive ω' near the edge of the balance drum, even though the fluid whirl is below shaft speed. This cannot be accounted for in the one-dimensional model and must be attributed to the two-dimensional character of the flow as it turns into the annular seal.

ANNULUS FLOW

As previously discussed, some rotor dynamicists have used an assumed whirl profile along the seal clearance, and one the main objectives of the present work was to investigate the form of the actual profile. Initial experiments were therefore carried out in a concentric system with and without shaft rotation, and with and without inlet whirl. The assumption of a whirl profile with no angular variation can be strictly true only in the concentric case, but it has been extended to eccentric cases where the short bearing theory could normally be justified. The second aim of the work was to test the validity of this extension by measuring the tangential and axial velocity components at a large number of points in the eccentric annulus.

ANNULUS TEST RIG

Fig. 9 shows the test rig used to study the behaviour of whirling flow in an annulus. The arrangements for controlling the leakage flow rate and the inlet whirl are broadly similar to those used in the radial flow rig, but access to the flow for LDA measurements is more troublesome. A narrow window was fitted along the length of the plain stator and a precision glass tube mounted in roller bearings was used to represent the shaft. It was driven at one end, leaving the other end open for an angled mirror to be inserted. Thus the optical axis is folded, with the transmission radial and the collection axial. A frequency shifter was used to resolve low velocities. The rotor diameter is 92mm and measurements were made over 140mm axial length. The mean radial clearance is 10mm which is clearly very large in comparison with real seals but the Reynolds number and the inlet whirl ratio are however comparable with values

in actual machines.

Two series of tests have been carried out, one series with the rotor and stator concentric, and the other at 50% eccentricity. Measurements were made at six angular positions in the eccentric cases.

RESULTS

Results from some concentric tests are shown in Figs.10 and 11 where measures of tangential velocity are plotted against axial position along the annulus for fixed flow rates. The data for Fig.10 was obtained with the shaft stationary, so the tangential velocity is usefully expressed in terms of the mean axial velocity U for a number of inlet whirl conditions which are quantified by the ratio of the flow passing through the swirl inducer Qs to the total flow Qt. The axial Reynolds number ($2Uh/\nu$) is 3150. The curves for higher whirl show the expected trend downwards towards zero. The apparent rise along parts of the lower curves is almost certainly due to radial shift of the maximum in the whirl distribution which has been measured in detail in some of the tests.

In Fig.11 the whirl ratio is plotted for a series of tests in which the inlet whirl was varied while the shaft speed was held at 295rev/min and the axial Reynolds number was 2650. The data can be simply tested for exponential behaviour by supposing that it can be described by the equation:

$$(\omega_x-\omega_\infty)/(\omega_0 - \omega_\infty)= \exp(-ax) \qquad (15)$$

where ω_∞ is the limiting angular velocity as x tends to infinity. Taking x as the test section length L, equation (15) can be written as:

$$\omega_L= C\omega_0+ (1-C)\omega_\infty \quad \text{where} \quad C = \exp(-aL). \qquad (16)$$

When data from Fig.11 is plotted as ω_L/Ω against ω_0/Ω, the points lie closely about a straight line from which estimates of C and ω_∞ can be derived:

$$\omega_\infty/\Omega = 0.4 \quad \text{and} \quad C = 0.42.$$

A limiting whirl ratio below 0.5 fits the fact that the stator surface is rougher than the good optical finish on the glass rotor. The value of C implies that, in the present case, departures from the limiting whirl ratio would decrease by a factor of ten for each 300mm of axial length.

Results for the eccentric cases are not yet fully analysed, but early indications are that the distributions of whirl and axial velocity are rather complex.

CONCLUSIONS

It has been demonstrated experimentally that the leakage flow between impeller shroud and pump casing can result in a whirl velocity at the seal inlet much greater than half shaft speed. A one-dimensional theory can model the general behaviour of the flow with empirically determined friction factors.

Different stator surface modifications were tested and radial grooves were found to be an effective whirl-control device. However, one effect of reducing the whirl of the radial inflow will be to increase the pressure at the seal entry. The leakage will therefore tend to increase and the whirl will consequently increase. This self-compensating effect of attempts to reduce the whirl can be minimised by concentrating efforts to modify the flow in the region just before the flow enters the seal.

In the concentric annulus flows so far tested, the influence of the inlet whirl persisted along the length of the test section and could be described quite well by an exponential approach to a limiting value.

REFERENCES

(1) Black HF, Allaire PE & Barrett LE
Inlet flow swirl in short turbulent annular seal dynamics.
9th Int Conf on Fluid Sealing, 141-152, BHRA 1981.

(2) Ehrich F & Childs D
Self-excited vibration in high-performance turbomachinery.
Mechanical Engineering, 66-79, May 1984.

(3) Kirk RG
A method for calculating seal inlet swirl velocity.
Rotating Machinery Dynamics, vol 2, ASME DE-vol 2, 1987.

(4) Kirk RG, Hustak JF & Schoeneck KA
Evaluation of liquid and gas seals for improved design of turbomachinery.
Proc Int Conf on Vibrations in Rotating Machinery, 387-394, IMechE 1988.

(5) Benckert H & Wachter J
Flow-induced spring coefficients of labyrinth seals for application in rotor dynamics.
NASA CP 2133, Proc of Wkshp at Texas A&M Univ, Rotordynamic problems of high performance turbomachinery, May 1980, 189-212.

(6) Hart JA & Brown RD
The use of fluid swirl to control the vibration behaviour of rotating machines.
Proc Int Conf on Vibrations in Rotating Machinery, 69-75, IMechE September 1988.

(7) Childs DW & Ramsey C
Seal-rotordynamic-coefficient test results for a model SSME ADT-HPFTP turbine interstage seal with and without a swirl brake.
NASA CP 3122, Proc of Wkshp at Texas A&M Univ, Rotordynamic instability problems in high performance turbomachinery, May 1990, 179-190.

(8) Tam LT, Przekwas AJ, Muszynska A, Hendricks RC, Braun MJ & Mullen RL
Numerical and analytical study of fluid dynamic forces in seals and bearings.
J Vibration and Acoustics, Stress and Reliability in Design, 315-325, vol 110, July 1988.

(9) Baskharone EA & Hensel SJ
A new model for leakage prediction in shrouded-impeller turbopumps.
Trans ASME, Vol 111, 118-122, June 1989.

(10) Williams M, Chen WC, Baché G & Eastland A
An analysis methodology for internal swirling flowsystems with a rotating wall.
J of Turbomachinery,83-90,vol 113, Jan 1991 Trans ASME

(11) Addlesee AJ & Altiparmak D
Factors influencing whirl at entry to balance drum seals in pumps.
Proc of Conf on Vibrations in Centrifugal Pumps, IMechE 1990, 33-40.

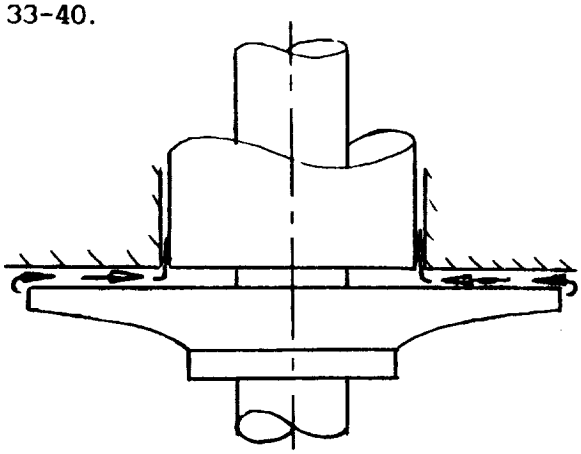

Fig.1 Diagram of leakage path.

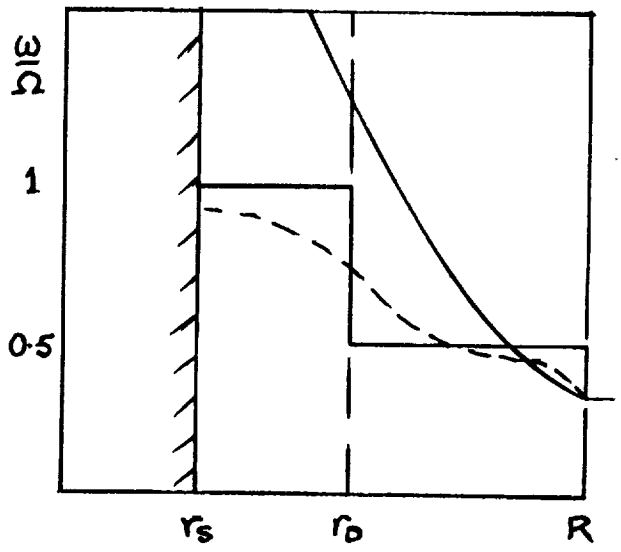

Fig.2 Types of whirl profile.

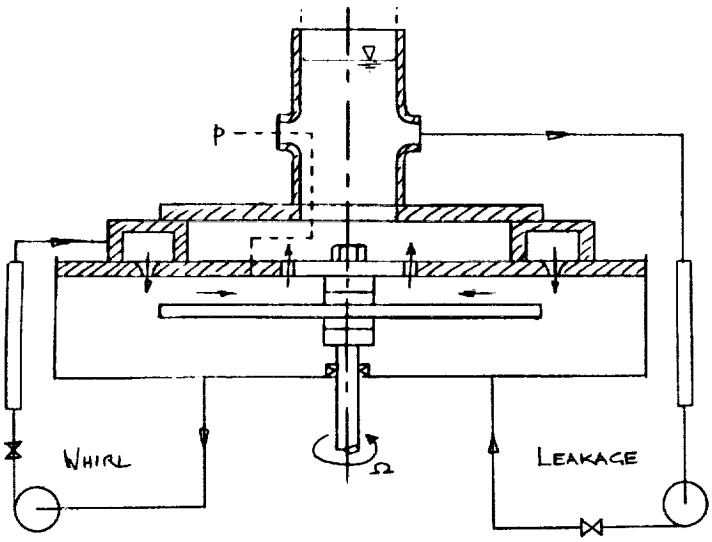

Fig. 3 Radial flow rig.

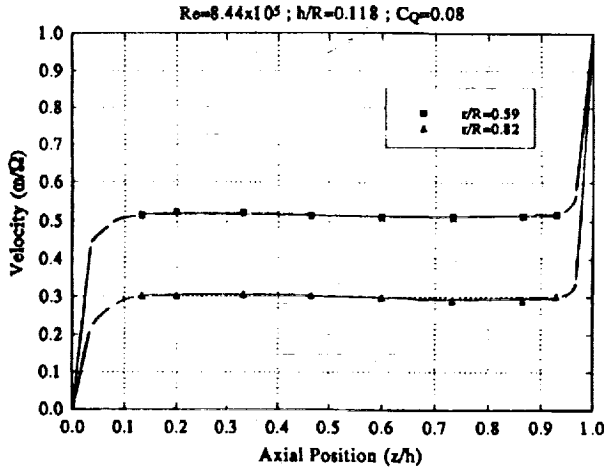

Fig. 4 Axial variation of whirl.

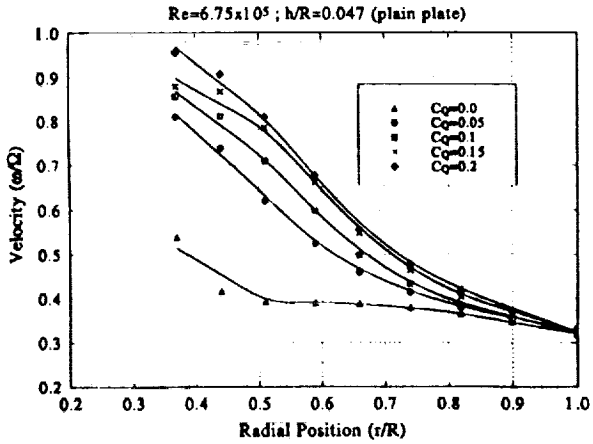

Fig. 5 Radial variation of whirl.

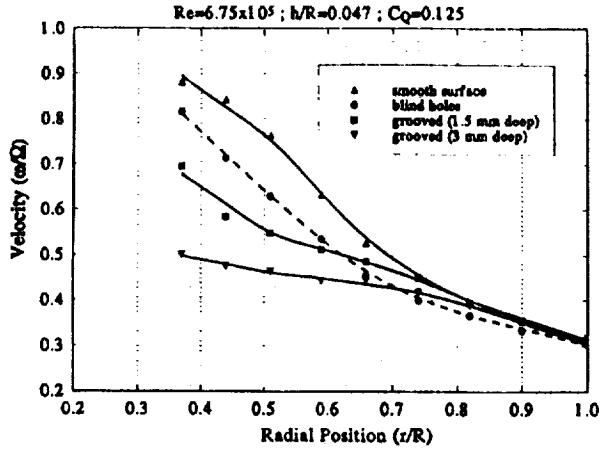

Fig.6 Whirl profiles for different stator surfaces.

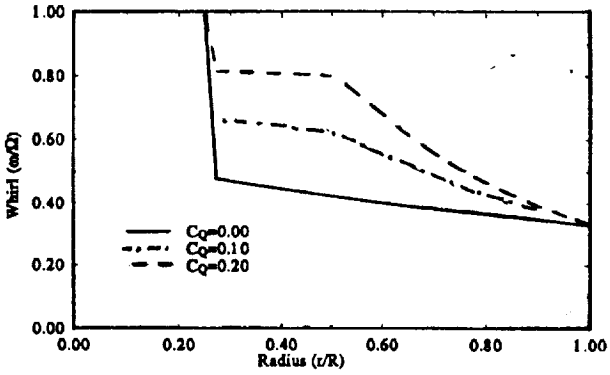

Fig.7 Theoretical whirl profiles for test rig.

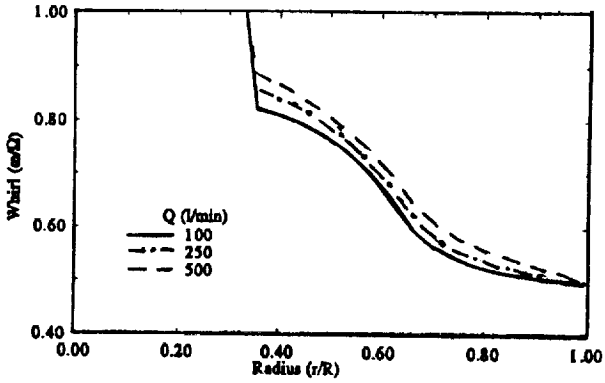

Fig.8 Theoretical whirl profiles for pump.

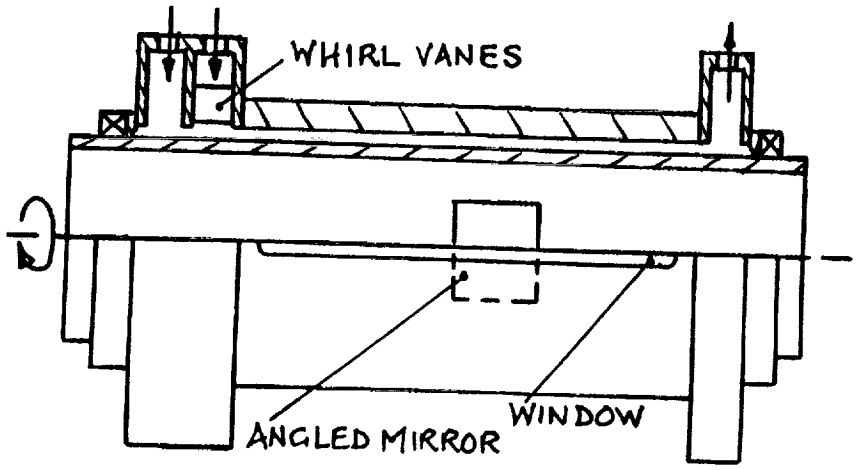

Fig. 9 Annulus test rig.

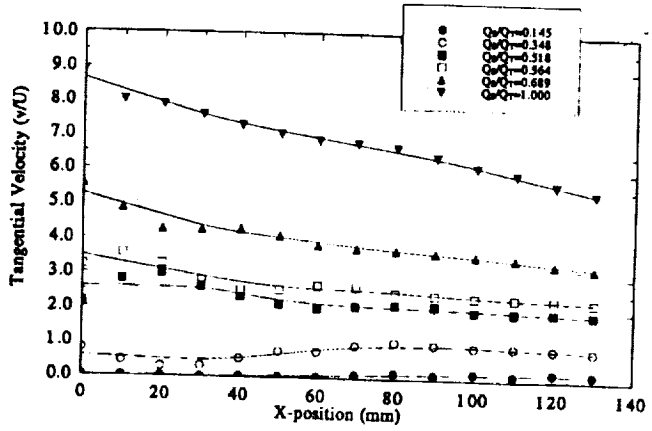

Fig. 10 Tangential velocity variation along a fixed annulus.

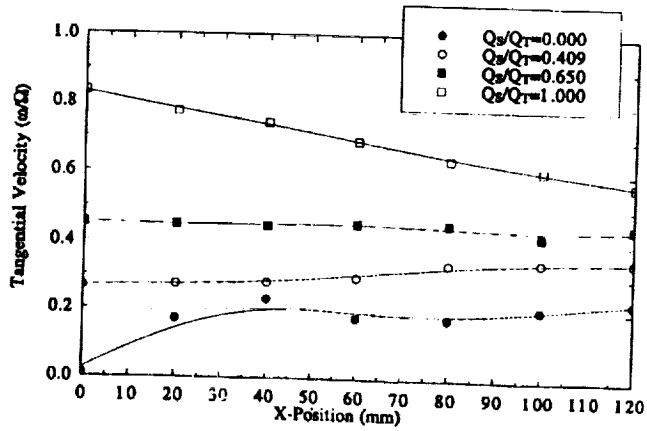

Fig. 11 Whirl variation along annulus with rotating shaft.